*Kidney International, Vol. 66 (2004), pp. 1826–1837*

# Gene expression profiling of anti-GBM glomerulonephritis model: The role of NF-κB in immune complex kidney disease

**Ju Han Kim,[1] Il Soo Ha,[1] Chang-Il Hwang, Young-Ju Lee, Jihoon Kim, Seung-Hee Yang, Yon Su Kim, Yun Anna Cao, Sangdun Choi, and Woong-Yang Park**

*Seoul National University Biomedical Informatics (SNUBI); Department of Pediatrics; Department of Biochemistry and Molecular Biology; Department of Internal Medicine, Seoul National University College of Medicine, Seoul, Korea; and Division of Biology, California Institute of Technology, Pasadena, California*

**Gene expression profiling of anti-GBM glomerulonephritis model: The role of NF-κB in immune complex kidney disease.**

*Background.* Immune complexes may cause an irreversible onset of chronic renal disease. Most patients with chronic renal disease undergo a final common pathway, marked by glomerulosclerosis and interstitial fibrosis. We attempted to draw a molecular map of anti-glomerular basement membrane (GBM) glomerulonephritis in mice using oligonucleotide microarray technology.

*Methods.* Kidneys were harvested at days 1, 3, 7, 11, and 16 after inducing glomerulonephritis by using anti-GBM antibody. In parallel with examining the biochemical and histologic changes, gene expression profiles were acquired against five pooled control kidneys. Gene expression levels were cross-validated by either reverse transcription-polymerase chain reaction (RT-PCR), real-time PCR, or immunohistochemistry.

*Results.* Pathologic changes in anti-GBM glomerulonephritis were confirmed in both BALB/c and C57BL/6 strains. Among the 13,680 spotted 65mer oligonucleotides, 1112 genes showing significant temporal patterns by permutation analysis of variance (ANOVA) with multiple testing correction [false discovery ratio (FDR) < 0.05] were chosen for cluster analysis. From the expression profile, acute inflammatory reactions characterized by the elevation of various cytokines, including interleukin (IL)-1 and IL-6, were identified within 3 days of disease onset. After 7 days, tissue remodeling response was prominent with highly induced extracellular-matrix (ECM) genes. Although cytokines related to lymphocyte activation were not detected, monocyte or mesangial cell proliferation-related genes were increased. Tumor necrosis factor-α (TNF-α) and nuclear factor-κB (NF-κB) pathway were consistently activated along the entire disease progression, inducing various target genes like complement 3, IL-1b, IL-6, Traf1, and Saa1.

*Conclusion.* We made a large-scale gene expression time table for mouse anti-GBM glomerulonephritis model, providing a comprehensive overview on the mechanism governing the initiation and the progression of inflammatory renal disease.

[1]These two authors contributed equally to this work.

**Key words:** Anti-GBM glomerulonephritis, microarray, NF-κB, mesangial cell, pathway analysis.

Received for publication October 29, 2003
and in revised form February 24, 2004, and May 10, 2004
Accepted for publication May 18, 2004



Large-scale gene expression analysis provides a logical approach in studying the detailed mechanisms behind the pathogenesis of various diseases. Using DNA microarray containing tens of thousands of genes, the genes regulating the key steps in disease initiation and progression can be identified [1]. The identification of specific genes involved in the pathogenesis of human diseases may reveal molecular targets for diagnosis and drug development [2]. As the clinical implications were evident in cancer patients [3], microarray can be applied to kidney diseases in classifying subsets of disease states with different clinical outcomes and in providing more efficient tools in clinical nephrology [4, 5].

Most glomerular disorders show a pattern of progressive decline in renal function with glomerulosclerosis and tubulointerstitial fibrosis [6]. The fibrotic change might serve as a final common pathway on the initial insults to glomeruli. A serial cascade of events triggered by certain stimuli (i.e., inflammation, nephrotoxic drugs, and ureteral obstruction) converge to a fibrogenic response in the glomerular and tubulointerstitial compartments of kidney. If we can address the pathogenesis of the fibrogenic process in terms of target molecules, it will cover the glomerulotubulointerstitial interplay. To this date, extensive researches have focused on listing the total transcripts involved in the development of various nephropathies in order to find genes that may be potentially involved in the pathogenesis [7–10]. Yano et al [9] compared the expression profile of 18,326 genes in primary human proliferating mesangial cells with IgA nephropathy to that in the control subjects and listed 203 human transcripts related to IgA nephropathy.

In the present study, we measured genome-wide gene expression levels in renal tissues of anti-glomerular basement membrane (GBM) glomerulonephritis model using oligonucleotide microarray technology. The roles of recruit and resident cells in the production of cytokines, growth factors, and extracellular matrix (ECM) components were systematically investigated. The major role of nuclear factor-κB (NF-κB) was suggested to be in the regulation of inflammatory as well as fibrogenic responses of the anti-GBM glomerulonephritis model system.

## METHODS

### Anti-GBM glomerulonephritis model

Basically we followed the previously described method to make anti-GBM glomerulonephritis model [11]. Briefly, GBM protein was extracted from rat kidneys and immunized to New Zealand White rabbits to raise anti-GBM antibody. The rabbit sera were heat-inactivated and immunoglobulin (Ig) fractions were isolated by protein A columns (Pierce, Rockford, IL, USA). Nephritis was induced by intravenous injection of 0.3 mg/g weight of rabbit anti-GBM IgG in 6-week-old female mice of BALB/c and C57BL/6 strains ($N = 20$ in each strain). Four mice at a time were sacrificed from each strain serially on days 1, 3, 7, 11, and 16. Using metabolic cages, we collected 24-hour urines and measured body weights before sacrifice. One half of a kidney was processed for histologic and immunohistochemical studies and the remaining one and one half were used for enzyme-linked immunosorbent assay (ELISA) and DNA microarray. All animal experiments were conducted in accordance with the NIH Guide for the Care and Use of Laboratory Animals.

### Light microscopy

Formalin-fixed tissues were embedded in paraffin and 4 μm sections were stained with periodic acid-Schiff (PAS). The amount of glomerular collagen was graded in 30 glomeruli according to the guide (delete the space) lines provided by Kagami et al [12]: 0, no mesangial staining; 1, focally increased mesangial staining at less than 25%; 2, 25% to 50% of glomerular tuft stained; 3, 50% to 75% of glomerular tuft stained; and 4, more than 75% of glomerular tuft stained. Interstitial collagen was scored according to the guidelines provided by Yamamoto et al [13]: 0, normal; 1, less than 10% of the area involved; 2, 10% to 30% involved; 3, 30% to 50% involved; and 4, more than 50% involved.

### ELISA

Chopped cortical tissue was suspended in 1 mL of serum-free RPMI (Sigma Chemical Co., St. Louis, MO, USA) and incubated in 5% $CO_2$ at 37°C. After 48 hours, the conditioned media were collected, mixed with proteinase inhibitors [phenylmethylsulfonyl fluoride (PMSF), aprotinin, leupeptin, and pepstatin A], and stored at −70°C until analysis. Fibronectin concentration was quantified by competitive inhibitory ELISA as described previously [14]. Total protein concentration was measured by BCA protein assay kit (Pierce). Transforming growth factor-β1 (TGF-β1) level in the urine was measured by ELISA (Quantikine human TGF-β1) (R&D Systems, Minneapolis, MN, USA) after activation of the latent TGF-β1 with 1 N HCl and neutralization with 1.2 N NaOH/0.5 mol HEPES. Serum and urinary creatinine were measured by alkaline picrate method as mg/mL (Sigma Chemical Co.). Fibronectin/total protein ratios in conditioned media and urinary TGF-β1/creatinine ratios were calculated as μg/mg and pg/mg, respectively.

### Oligonucleotide microarray

Pooled total RNA from five control mice were used as the reference group in all experiments. Three out of the four RNAs extracted from anti-GBM glomerulonephritis mice each at days 1, 3, 7, 11, and 16 were used for triplicate experiments at each five time points. Total RNA was prepared by using TriZol reagent (Life Technologies, Gaithersburg, MD, USA). The array used in this experiment was the Caltech 16K Custom-Oligo array. The oligonucleotide probes were purchased from Operon Technologies (Alameda, CA, USA) (70-mer) and Compugen-Sigma-Genosys (Jamesburg, NJ, USA) (65-mer) and inkjet printed by Agilent Technologies (Palo Alto, CA, USA). First and second strand cDNA synthesis was initiated by incubating 5 μg of total RNA with 5 μL of T7 promoter primer in nuclease-free water at 65°C for 10 minutes. Fluorescent Linear Amplification Kit (Agilent Technologies) was used [15]. Briefly, the resulting mixture was incubated with 4 μL of 5× first strand buffer, 2 μL of 0.1 mol/L dithiothreitol (DTT), 1 μL of 10 mmol/L deoxynucleoside triphosphate (dNTP), 1 μL of 200 ng/μL random hexamers, 1 μL of 200 U/μL Moloney-murine leukemia virus-reverse transcription (MMLV-RT), 0.5 μL of 40 U/μL RnaseOUT, and 1 μL of Triton X-100 at 40°C for 4 hours. After cDNA synthesis, the sample was in vitro transcribed and labeled by incubating it with 4 μL of cyanine-3 (Cy3)-CTP (6.0 mmol/L) (Perkin Elmer Life Sciences, Norwalk, CT, USA) or 4 μL of cyanine-5 (Cy5)-CTP (4.0 mmol/L) (Perkin Elmer Life Sciences), 20 μL of transcription buffer, 8 μL of NTP mixture, 6 μL of 0.1 mol/L DTT, 0.5 μL of RnaseOUT, 0.6 μL of inorganic pyrophosphatase, 0.8 μL of T7 RNA polymerase, and 20.1 μL of nuclease-free water at 40°C for 3 hours. Before hybridization, 8 μg of Cy3-CTP–labeled cRNA and 8 μg of Cy5-CTP–labeled cRNA were mixed together with 2.5 μL of Mouse Cot-1 DNA (Invitrogen, Carlsbad, CA, USA), 2.5 μL of

deposition control target (Operon Technologies), and 12.5 μL of 2× hybridization buffer (Agilent Technologies). The mixture was centrifuged at 12,000 rpm for 3 minutes after it was boiled for 2 minutes. About 24 μL of the mixture was hybridized on the array at 65°C for 16 hours. After hybridization, the array was washed with solution I [0.5× standard sodium citrate (SSC), 0.01% sodium dodecyl sulfate (SDS), and 1 mmol/L DTT in nuclease-free water], solution II (0.25× SSC, 0.01% SDS, and 1 mmol/L DTT in nuclease-free water), and solution III (0.06× SSC and 1 mmol/L DTT in nuclease-free water), respectively. The arrays were scanned using the Agilent G2505A scanner (Agilent Technologies) and the array data were extracted using Agilent G2566AA Extraction Software version A.6.1.1 (Agilent Technologies).

### Data analysis

Fluorescence intensity was processed and measured using Agilent G2566AA Extraction Software version A.6.1.1. Intensity data were imported to an in-house microarray database. Variance stabilizing normalization by Huber et al [16] was applied with the "vsn" package in Bioconductor using the R statistical package. After performing intensity-dependent global LOWESS regression, spatial and intensity dependent effects were managed by pin group LOWESS normalization following by the approach of Yang et al [17]. F test for each probe was performed to discover the genes showing significant temporal patterns. It was suggested by our quantile-quantile plot analysis, however, that the normality assumption for the data set was not held [18] (see *http://www.snubi.org/publication/antiGBM/*). Residual quantiles were deviated from the theoretic quantiles. Since the distributions of the observed statistics are unknown, an empiric reference set was generated by permuting the sample labels. For each probe, we randomly permuted 100,800 times, following the rationale of Dwass [19], out of the theoretic 168,168,138 exact ways of assigning 15 objects to five groups with triplicates (i.e., $15!/(3!)^{15}$). Then $P$ value for each probe was calculated as the rank of the observed statistic, $F_i$, among the empiric distributions divided by the permutation size. To manage the multiple hypothesis testing problem, the $P$ value cutoff was decided by determining the false discovery rate (FDR) following the scheme of Storey and Tibshirani [20]. FDR is the proportion of false positives among all genes called significant. Hence, the estimated number of false positives in the present study is presumed to be about 55 out of the 1112 genes called significant at FDR < 0.05. Cluster analysis was performed for the 1112 (FDR < 0.05) genes having significant temporal patterns by MITree-*K* partitional clustering algorithm [21] (*http://www.snubi.org/software/MITree/*). The cluster analysis result with full annotations is provided at our supplement web page (Data A at *http://www.snubi.org/publication/antiGBM/*). Clusters were mapped onto biologic pathways and sorted on the order of matching significance using ArrayXPath [22]. The gene expression data set was submitted to the Gene Expression Omnibus (*http://www.ncbi.nlm.nih.gov/geo/*) under the accession numbers, GSM15078-GSM-15029, GSE954-GSE958, and GSE969.

### Reverse transcription-polymerase chain reaction (RT-PCR) and real-time PCR

The first strand cDNA was synthesized from 1 μg of total RNA using reverse transcriptase and 1 μmol/L of oligo-dT primer. Each cDNA sample was amplified by using specific primers against complement component 3 (C3) (sense 5′-GTGACATCCCAGTCACA-3′ and antisense 5′-CTCAAACTCTGCGGAGA-3′), serum amyloid A1 (Saa1) (sense 5′-GTTCACGAGGCTTTCCA-3′ and antisense 5′-GTCAGGCAGTCCAGGA-3′), interleukin 1 beta (IL-1β) (sense 5′-AGAAGCTGTGGCAG CTA-3′ and antisense 5′-TGAGGTGCTGATGTACCA-3′), fibronectin 1 (Fn1) (sense 5′-GTGATCCCCATGAA GCAA-3′ and antisense 5′-AGGGTGACCAACTGT CA-3′), collagen, type III, alpha 1 (Col3α1) (sense 5′-AAAGAGGAGGTCCTGGAA-3′ and antisense 5′-CT TGCCAGGAGCACCA-3′), complement component 1, q subcomponent, alpha polypeptide (C1qα) (sense 5′-GT CGCTTCATCTGTGCA-3′ and antisense 5′-CGGGG ATCGTTTATTCCA-3′), complement component 1, q subcomponent, beta polypeptide (C1qβ) (sense 5′-GA CTACGGGGCTACACA-3′ and antisense 5′-GCAGT CAAGGGGGTGA-3′), complement component 1, q subcomponent, c polypeptide (C1qc) (sense 5′-AGGGC CGATACAAACAGA-3′ and antisense 5′-CCGATGG ATCAGGAACCA-3′), TGF-β1 (TGFβ1) (sense 5′-CTGCGCTTGCAGAGA-3′ and antisense 5′-CAGGGT CCCAGACAGA-3′), connective tissue growth factor (Ctgf) (sense 5′-CCAAGCAGCTGGGAGA-3′ and antisense 5′-TGCTTCTCCAGTCTGCA-3′), and glyceraldehyde-3-phosphate dehydrogenase (GAPDH) (sense 5′-ACCACAGTCCATGCCATCAC-3′ and antisense 5′-TCCACCACCCTGTTGCTGTA-3′). Specific bands were analyzed after agarose gel electrophoresis.

Real-time PCR was performed in a LightCycler using DNA Master SYBR Green I dye (Roche Molecular Biochemicals, Pleasanton, CA, USA). Measurements of the threshold cycles were made at the end of each extension step by the second-derivative method using LightCycler software version 4.0 (Roche Molecular Biochemicals). Melting curve analysis was performed to confirm the identity of peaks of interest in all samples. PCR-amplified fragments of the respective genes were cloned into pGEM easy T vector (Promega, Madison, WI, USA),

which was used as standard DNAs for quantification, and results were normalized with the amount of GAPDH mRNA.

### Immunofluorescence staining

For immunofluorescent staining of mouse kidney, tissue sections were fixed in formalin/phosphate-buffered saline (PBS) and embedded with paraffin. Visualization was performed using Cy3 antirabbit IgG (Jackson ImmunoResearch, West Grove, PA, USA) followed by fluorescence microscopy (Zeiss Axioplan using a Hamamatsu ORCA CCD camera). Briefly, tissues were fixed with 2% paraformaldehyde in PBS. After permeabilization using 0.5% NP-40, cells were blocked in 0.2% gelatin and 0.5% bovine serum albumin (BSA) in PBS. Primary anti-Traf1, anti-Traf2, and Traf-3 antibodies from Santa Cruz Biotechnologies (Santa Cruz, CA, USA) (1:200 dilution) were incubated with kidney tissues and Traf proteins were visualized using Cy5 antirabbit IgG (Jackson ImmunoResearch) and fluorescence microscopy (Zeiss).

## RESULTS

### Expression profile of anti-GBM glomerulonephritis

Following the previously described protocols [11], we made an anti-GBM glomerulonephritis model by injecting rabbit antirat GBM antibody into two strains of mouse, BALB/c and C57BL/c. Although these two were different in human leukocyte antigen (HLA) types (H-$2^b$ for C57BL/6 and H-$2^d$ for BALB/c), they responded to immune complex in the same manner and to similar extents. Edema, proteinunria and decreased serum protein levels appeared within the first day of disease induction in both strains (Fig. 1A). Moreover, signs of late changes like fibrogenic responses at around 7 to 11 days were apparent in both strains. We measured the mesangial matrix score as well as interstitial fibrosis score in PAS-stained kidney tissues (Fig. 1B and C). According to the serial changes in clinicopathologic findings, we divided the disease into two periods: a heterologous phase of acute glomerulonephritis at 1 to 3 days and a homologous phase with following glomerulosclerosis and tubulointerstitial fibrosis at 7 to 16 days. Along with the biochemical and histologic parameters, our anti-GBM model covers the entire disease span from acute glomerulonephritis to tubulointerstitial fibrosis. To draw a composite map of gene expression profiles using oligonucleotide microarray containing 13,618 mouse genes, we performed triplicate microarray experiments for anti-GBM glomerulonephritis model at days 1, 3, 7, 11, and 16 with 15 microarray slides.

We selected 1112 genes (6.89%) that showed significant temporal patterns across the time intervals by permutation analysis of variance (ANOVA) with multiple comparison and estimated FDR (<0.05). The expression profiles were divided into 50 clusters according to their temporal expression patterns (Data A at *http://www.snubi.org/publication/antiGBM/*). In the heterologous phase, the groups of genes related to acute phase reactants and cytokines were elevated as early as days 1 to 3, while a small portion of selected genes showed a gradual decrease in expression during this period. For example, several genes like potassium channels or aquaporins were decreased. After day 7 of the disease, the groups of genes related to immune response and fibrosis were increased during homologous phase. Transcripts of growth factors, channel protein and metabolic enzymes were decreased at around days 11 to 16. In addition, several unknown expressed sequence tags (ESTs) were markedly decreased in late phase. All these findings explain the major changes in pathologic examination as well as biochemical analysis.

After the gene expression profiles were clustered into 50 clusters, we mapped all microarray probe identifiers onto biologic pathways using ArrayXPath [22] (*http://www.snubi.org/software/ArrayXPath/*). The nonredundant 1260 BioCarta nodes in 277 murine pathways were 100% covered by our 18,326 probes. ArrayXPath successfully mapped 139 probe identifiers out of the 1112 members in the 50 clusters (12.5%) onto 209 BioCarta pathways (Data B at *http://www.snubi.org/software/ArrayXPath/ArrayXPath_antiGBM.html*).

In cluster 15, 89 genes were up-regulated slightly in days 1 and 3 and higher in days 7, 11, and 16. Among them, 13 genes could be successfully plotted onto BioCarta pathways. Especially five pathways like D4-GDI signaling pathway, T-cytotoxic cell surface molecule, T-helper cell surface molecule, effects of calciurenin in keratinocyte differentiation, and Fc epsilon receptor I signaling in mast cells showed statistically significant match to eight unique genes. Especially three genes (*Pla2g4a*, *Prkcb*, and *Fcer1g*) were related to the Fc epsilon receptor I signaling in mast cell while another four genes (*Mapk1*, *Hras1*, *Vav1*, and *Lyn*) for this pathway were also chosen in other clusters. Expression of *Pla2g4a* encoding cytosolic phospholipase $A_2$ plays an important role in eicosanoid metabolism and bleomycin-induced pulmonary fibrosis [23]. Cluster 45 showed highly elevated expression levels from days 3 to 7 and then moderately elevated levels after days 11 and 16. Five out of the 17 members were mapped onto pathways. Rac1 and Vav1 were commonly mapped onto many inflammatory pathways including Rac1 cell motility, T cell receptor, B cell receptor, and Ras-independent pathway in natural killer cell-mediated cytotoxicity. The genes in cluster 5 showed different expression pattern, which were moderately up-regulated in days 1 and 3, but afterwards down-regulated continuously. This cluster included proteolytic enzymes like kallikreins (i.e., Klk9, Klk13, Klk16, Klk21, and Klk27), Enpp1, Dpp7, Proc, Acp5, Cspg5, Dipep1, and receptors or transporters like Sigirr, Accn5, Fabp7, and Abcb1a.

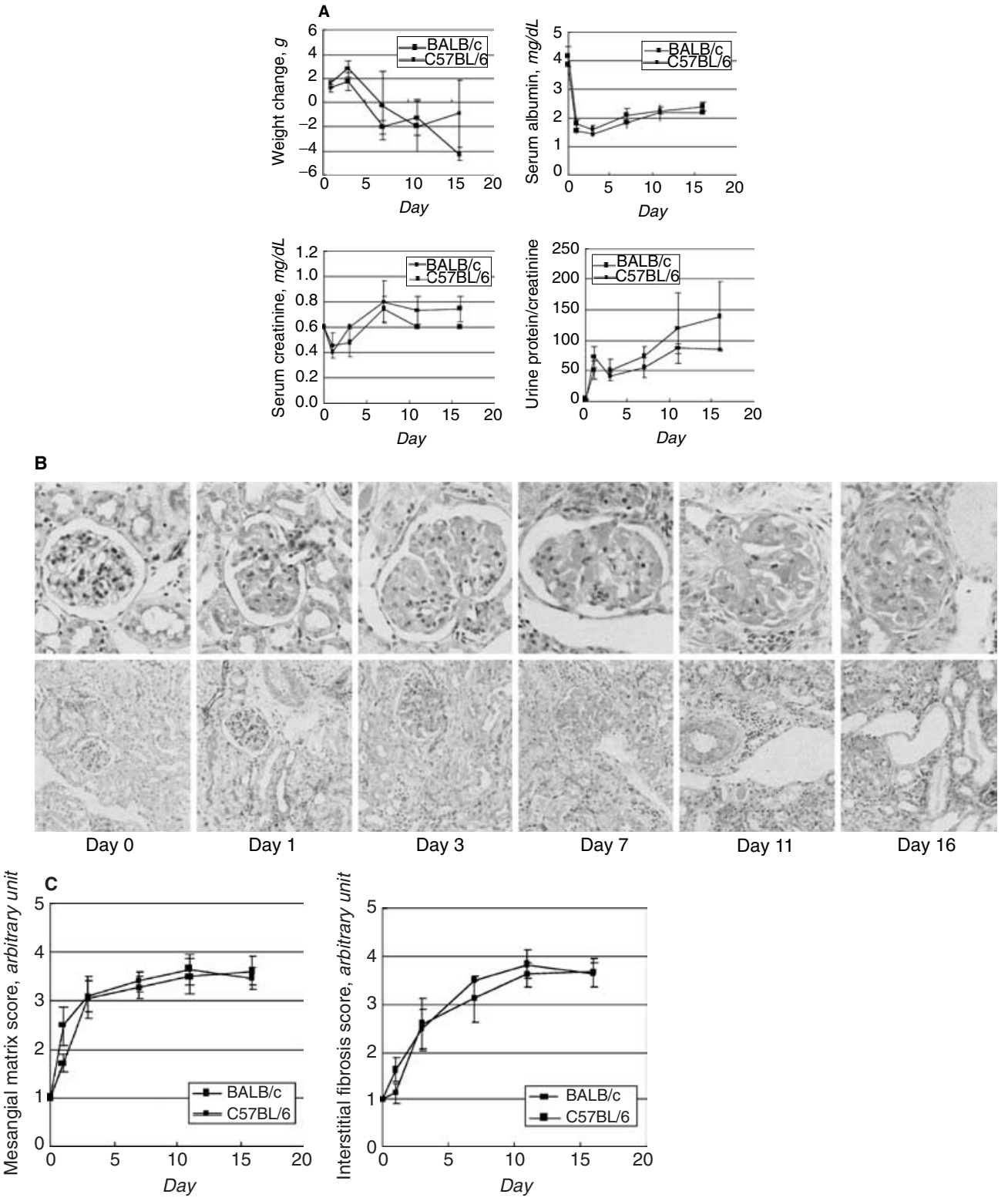


**Fig. 1. Biochemical and pathologic analysis on anti-glomerular basement membrane (GBM) glomerulonephritis model.** (*A*) Changes of body weights at each time point were monitored throughout the disease progression. The level of serum creatinine, serum proteins and urinary proteins were measured to calculate serum or urine protein/creatinine ratios. Each value is an average of four mice with error bar displaying the standard deviation. (*B*) Pathologic analysis showed marked changes in glomeruli (upper row) and interstitia (lower row) throughout the disease progression [periodic acid-Schiff (PAS) 400× for the glomeruli, 100× for the interstitial]. (*C*) The degree of pathologic changes could be transformed to parametric indices for mesangial matrix and interstitial fibrosis. Each value is averaged among four mice with error bar displaying the standard deviation.

**Table 1.** Expression profiles of cytokines

| Category | Symbol | Fold change (mean ± SD) | | | | |
|---|---|---|---|---|---|---|
| | | Day 1 | Day 3 | Day 7 | Day 11 | Day 16 |
| Fibrosis | | 0.931 ± 0.327 | 1.251 ± 0.056 | 1.942 ± 0.000 | 2.064 ± 0.071 | 1.994 ± 0.237 |
| | *Ctgf* | 1.969 ± 0.840 | 1.415 ± 0.512 | 1.337 ± 0.619 | 0.649 ± 0.961 | 0.804 ± 0.505 |
| | *Tgfβ1i4* | 0.025 ± 0.170 | 1.397 ± 0.303 | 1.332 ± 0.529 | 0.492 ± 0.338 | 0.802 ± 0.469 |
| | *Tgfβ1i1* | 0.516 ± 0.317 | 0.750 ± 0.180 | 0.791 ± 0.157 | 1.202 ± 0.176 | 0.755 ± 0.368 |
| | *Tgfβ1* | −0.221 ± 0.426 | ND | 0.456 ± 0.322 | ND | ND |
| Growth/apoptosis | *Tnfα* | −0.218 ± 0.428 | 0.317 ± 0.022 | 0.299 ± 0.193 | 0.267 ± 0.231 | −0.022 ± 0.141 |
| | *Pdgfa* | 0.121 ± 0.338 | 1.278 ± 0.120 | 0.907 ± 0.143 | 1.182 ± 0.104 | 0.306 ± 0.623 |
| | *Egf* | −0.434 ± 0.104 | −1.630 ± 0.251 | −2.318 ± 0.136 | −1.617 ± 0.221 | −1.702 ± 0.166 |
| Monocyte | *Scya2* | 0.499 ± 0.056 | 2.783 ± 0.052 | 2.699 ± 0.278 | 3.009 ± 0.151 | 3.025 ± 0.296 |
| | *IL-1β* | 0.537 ± 0.055 | 0.652 ± 0.016 | 0.851 ± 0.785 | 1.472 ± 0.264 | 1.626 ± 0.020 |
| | *IL-6* | 0.563 ± 0.036 | 1.300 ± 0.919 | 1.117 ± 0.789 | 2.722 ± 0.094 | 2.140 ± 1.513 |
| | *Scya6* | ND | 0.352 ± 0.250 | 1.529 ± 0.964 | 1.063 ± 0.164 | 2.031 ± 0.452 |
| | *Gcr1* | ND | 1.319 ± 0.932 | 1.786 ± 0.110 | 1.366 ± 0.558 | 1.878 ± 0.545 |
| | *Scya5* | 0.385 ± 0.353 | 1.144 ± 0.004 | 1.274 ± 0.066 | 1.091 ± 0.268 | 0.479 ± 0.153 |
| | *Ccr5* | 1.036 ± 0.599 | 1.422 ± 1.006 | 1.880 ± 0.310 | 1.916 ± 0.173 | 1.821 ± 0.229 |
| T cell/B cell | *Tnfsf5* | 0.179 ± 0.208 | 0.245 ± 0.276 | 0.779 ± 0.016 | 0.652 ± 0.242 | −0.113 ± 0.110 |
| | *IL-2* | 0.405 ± 0.182 | 0.082 ± 0.062 | −0.055 ± 0.348 | −0.369 ± 0.087 | −0.092 ± 0.177 |
| | *IL-10* | 0.212 ± 0.170 | −0.261 ± 0.185 | −0.482 ± 0.340 | −0.514 ± 0.304 | 0.671 ± 0.001 |
| | *IL-4* | ND | 0.219 ± 0.154 | 0.369 ± 0.261 | 0.359 ± 0.208 | ND |
| | *IL-17* | −0.538 ± 0.175 | −0.639 ± 0.063 | −0.957 ± 0.312 | −1.212 ± 0.101 | 0.576 ± 0.613 |
| | *IL-18* | −0.068 ± 0.040 | −0.036 ± 0.088 | −0.215 ± 0.048 | 0.061 ± 0.198 | 0.365 ± 0.133 |
| | *IL-15* | −0.827 ± 0.071 | −1.078 ± 0.156 | −1.549 ± 0.118 | −1.336 ± 0.248 | −1.626 ± 0.108 |
| | *IL-5* | −0.413 ± 0.081 | −0.104 ± 0.185 | 0.291 ± 0.319 | 0.023 ± 0.134 | 0.016 ± 0.062 |

### Inflammatory cytokines related to monocyte activation

In this immune complex disease model, we focused on the changes of total cytokines presented in our array. We found patterns of immune responses through the gene expression profiles. As shown in Table 1, we categorized cytokines in four groups: those related to fibrosis, growth/apoptosis, monocyte, and lymphocyte. Members of the growth/apoptosis cytokines such as epidermal growth factor (EGF) [24], insulin-like growth factor-1 (IGF-1) [25], and interleukins like IL-15 [26] were down-regulated. These cytokines were previously proven to be involved in renal diseases and may be good therapeutic targets for minimizing fibrogenic effects in renal disease patients.

We looked for evidences of mesangial cell activation by recording the elevation of monocyte cytokines such as tumor necrosis factor-alpha (TNF-α), chemokine receptors (Ccr1 and Ccr5), small inducible cytokine family [monocyte chemoattractant protein-1 (MCP-1), regulated upon activation, normal T cell expressed and secreted (RANTES), and multidrug resistance-associated peptide (MRP1)] and interleukins (IL-1β and IL-6). However, interleukins involved in the stimulation of T or B lymphocytes were not increased in this model, while some of interleukins like IL-15 were decreased.

### Glomerulosclerosis and interstitial fibrosis

The expression of cytokines plays a critical role during the pathogenesis of inflammatory kidney disease, which is involved in tissue remodeling and repair by increasing ECM components. One of the most extensively investigated cytokines in the context of renal disease is TGF-β [27, 28]. In our microarray experiment, the transcript of TGF-β1 was not detected more than two fold of baseline (Table 1). However, we confirmed increased urinary excretion of TGF-β1 as measured by ELISA (Fig. 2A) and up-regulation in renal tissue by RT-PCR (Fig. 2B). The evidence for the presence of TGF-β1 in inflammatory renal disease was supported by the elevation of target genes like *Tgfbi*, T*gfb1i1*, and *Tgfb1i4* (Table 1). Connective tissue growth factor (CTGF) has been suggested to induce interstitial fibrosis directed by TGF-β1 [29]. In this study, CTGF was expressed as early as the first day of disease induction preceding TGF-β1 expression, which means that it might also be involved in inflammatory responses (Table 1) (Fig. 2B).

After 11 days of the disease, ECM proteins were accumulated in the glomeruli and interstitia (Fig. 1B). Fn1 and collagen type III isotype alpha1 (Col3α1) were elevated in the affected kidney beginning from day 7 as observed through microarray analysis (Fig. 2C). We confirmed the expression changes of Fn1 and Col3α1 by RT-PCR (Fig. 2B) and immunofluorescence staining (Fig. 2D).

### NF-κB–mediated gene expression

One of the major culprits of anti-GBM glomerulonephritis is NF-κB, which can modulate inflammatory responses in various diseases. Target genes for NF-κB were marked elevated at any time points in this model, either. While some of them were elevated at a

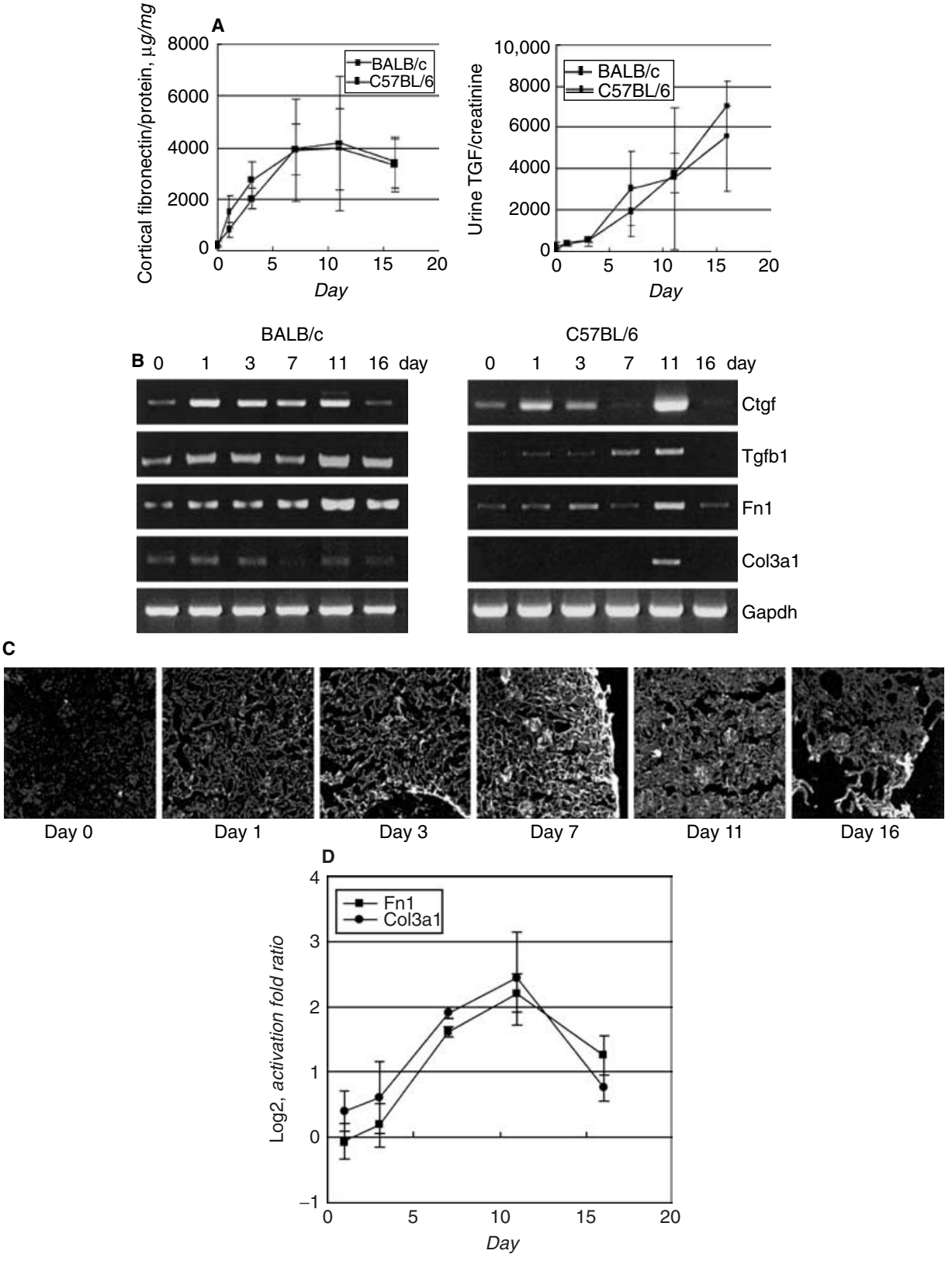


**Fig. 2. Molecular changes related to glomeruloscerosis or interstitial fibrosis.** (*A*) The protein levels of urinary transforming growth factor-β (TGF-β1) and renal parenchymal fibronectin were measured by enzyme-linked immunosorbent assay (ELISA). Each value is an average of four mice with error bar displaying the standard deviation. (*B*) The transcript levels of *Tgfβ1*, *Ctgf*, *Fn1*, and *Col3α1* at indicated time points were analyzed by reverse transcription-polymerase chain reaction (RT-PCR) using total RNA from BALB/c and C57BL/6. (*C*) Using immunofluorescence analysis, the level of Col3α1 in C57BL/c mouse renal cortex was monitored (100×). (*D*) $Log_2$ transformed ratio of Fn1 and Col3α1 in DNA microarray was plotted with standard deviation ($N = 3$).

**Table 2.** Gene expression profiles of nuclear factor-κB (NF-κB) and its target genes

| Category | Symbol | Fold change (mean ± SD) | | | | |
|---|---|---|---|---|---|---|
| | | Day 1 | Day 3 | Day 7 | Day 11 | Day 16 |
| Acute, sustained | *Saa1* | 3.249 ± 0.635 | 3.314 ± 0.304 | 3.096 ± 0.427 | 2.494 ± 0.564 | 1.949 ± 0.955 |
| | *Egr1* | 1.760 ± 0.315 | 2.252 ± 0.537 | 2.743 ± 0.255 | 2.688 ± 0.091 | 2.262 ± 0.326 |
| | *Birc5* | 1.544 ± 0.017 | 2.015 ± 0.123 | 1.780 ± 0.138 | 1.695 ± 0.069 | 1.571 ± 0.107 |
| Early, transient | *Nfκb* | 0.460 ± 0.261 | 1.245 ± 0.039 | 1.153 ± 0.113 | 0.672 ± 0.053 | 0.491 ± 0.105 |
| | *Ptgs2* | 0.381 ± 0.221 | 1.588 ± 1.122 | 0.277 ± 0.196 | 0.922 ± 0.623 | 0.604 ± 0.235 |
| | *Rel* | 0.519 ± 0.188 | 1.422 ± 0.273 | 1.274 ± 0.025 | 1.509 ± 0.201 | 0.822 ± 0.179 |
| | *Traf1* | 0.521 ± 0.219 | 1.125 ± 0.146 | 0.971 ± 0.071 | 0.847 ± 0.203 | 0.097 ± 0.128 |
| | *Irf1* | 0.250 ± 0.137 | 1.242 ± 0.006 | 1.170 ± 0.095 | 1.026 ± 0.227 | 0.913 ± 0.183 |
| Early, sustained | *Atf3* | 0.938 ± 0.177 | 1.806 ± 0.035 | 1.800 ± 0.115 | 1.741 ± 0.081 | 1.717 ± 0.036 |
| | *Birc2* | 0.268 ± 0.242 | 1.336 ± 0.179 | 1.917 ± 0.027 | 1.812 ± 0.127 | 1.586 ± 0.273 |
| | *C3* | 0.870 ± 0.563 | 1.512 ± 0.157 | 2.307 ± 0.323 | 2.160 ± 0.967 | 1.881 ± 0.014 |
| | *Crol* | 0.296 ± 0.568 | 2.408 ± 0.244 | 2.196 ± 0.323 | 1.913 ± 0.095 | 1.762 ± 0.812 |
| | *Junb* | 1.021 ± 0.146 | 2.473 ± 0.306 | 3.008 ± 0.156 | 2.779 ± 0.227 | 2.301 ± 0.244 |
| | *Myc* | 0.027 ± 0.225 | 2.174 ± 0.583 | 2.706 ± 0.089 | 2.249 ± 0.348 | 2.249 ± 0.320 |
| | *Trl2* | 0.017 ± 0.273 | 1.903 ± 0.053 | 2.417 ± 0.157 | 2.259 ± 0.154 | 2.118 ± 0.446 |
| | *Bcl3* | 0.150 ± 0.193 | 2.096 ± 0.319 | 2.119 ± 0.869 | 2.261 ± 0.140 | 2.300 ± 0.302 |
| | *Vcam1* | 0.250 ± 0.061 | 2.303 ± 0.211 | 2.717 ± 0.081 | 3.118 ± 0.335 | 2.124 ± 0.410 |
| | *Scay2* | −0.701 ± 0.101 | 1.681 ± 0.058 | 2.258 ± 0.156 | 2.515 ± 0.381 | 1.955 ± 0.227 |
| Late | *Mekk1* | 0.268 ± 0.029 | 0.915 ± 0.359 | 1.329 ± 0.045 | 1.459 ± 0.264 | 1.148 ± 0.512 |
| | *Bcl2a1c* | 0.094 ± 0.234 | 0.534 ± 0.642 | 1.268 ± 0.033 | 1.893 ± 0.201 | 2.057 ± 0.557 |
| | *Bcl2a1d* | −0.118 ± 0.055 | 0.102 ± 0.752 | 0.949 ± 0.004 | 1.907 ± 0.232 | 1.932 ± 0.379 |
| | *IL-1*β | 1.184 ± 0.366 | 0.965 ± 0.798 | 1.806 ± 0.263 | 1.691 ± 0.009 | 1.909 ± 0.029 |
| | *IL-6* | 0.563 ± 0.325 | 1.300 ± 0.919 | 1.117 ± 0.789 | 2.722 ± 0.094 | 2.140 ± 1.513 |

specific time point, NF-κB seemed to work all through the disease course (Table 2). Within 24 hours, acute phase reactants like serum amyloid proteins (Saa1) and early growth response 1 (Egr1) were increased. These genes might be transcribed upon immune complex deposition in the glomeruli through the activation of endogenous nuclear factors and other NF-κB target genes. Signals inducing those target genes can also up-regulate new sets of NF-κB and rel oncogene (Rel) transiently at day 3, which might be involved in the maintenance of target genes. Spikes of NF-κB and Rel transcription may possibly induce other transcription factors like ATF-3, Jun-B, and Myc, which eventually lead to late phase responses such as interstitial fibrosis and tissue remodeling. Interestingly, NF-κB at late phase directed the transcription of antiapoptotic genes like *BCL3*, *MEKK1*, *Bcl1a1c*, and *Bcl2a1d*, which suggest that the induction of NF-κB may prevent tissue destruction. We confirmed the expression of *IL-1*β, *IL6*, *Saa1*, and *C3* genes by RT-PCR in both strains (Fig. 3A). In addition, we performed real-time RT-PCR analysis for IL-1β in parallel to crosscheck the microarray data by different platform.

As a target for NF-κB, we found that series of complements were up-regulated in our model. Renal parenchymal cells expressed the complements because we perfused mouse kidney to remove any circulating cells (Table 2) (Fig. 4). Specifically, *C1qa*, *C1qb*, *C1qc*, and *C3* were expressed at day 11. We confirmed those findings by performing RT-PCR for both strains of mice (Fig. 4A). We also counted the copy number of C1qc transcript using real-time RT-PCR method, which also showed consistent pattern in the sequential changes of *C1qc* gene in both strains (Fig. 4B)

We also focused on Traf family genes that transduce the signaling from TNF to NF-κB and are bona fide targets of NF-κB by positive feedback. In spite of the weak increase in transcript messages of Traf1 in both RT-PCR and microarray (Fig. 5A and B), the signal of the Traf1 protein was quite high in the glomeruli of disease kidney (Fig. 5C). Traf2 and Traf3 were also increased in our model at later phases, but present in a weaker signal as observed from immunofluorescence staining.

## DISCUSSION

While the anti-GBM model is a well-known system for the renal disease progression, we made an effort to understand the disease in view of the complete transcriptomic map using 13,680 mouse genes. We monitored the temporal changes in gene expression together with clinicopathologic variables in the same mouse. Previous studies on RNA expression in experimental kidney disease have shown that renal mRNA levels for ECM components and cytokines can be used as a prognostic marker [5, 30]. Our results lead to the composition of more intensive maps with multiple parameters. From this data, we found the central role of monocytes, but not lymphocytes, in the progression of our renal disease model. NF-κB might play an important role in directing responses to the immune complex of the glomerulus.

One of the key components responsible for directing the final common pathway of fibrotic responses in inflammatory nephropathy might be TGF-β1 and its

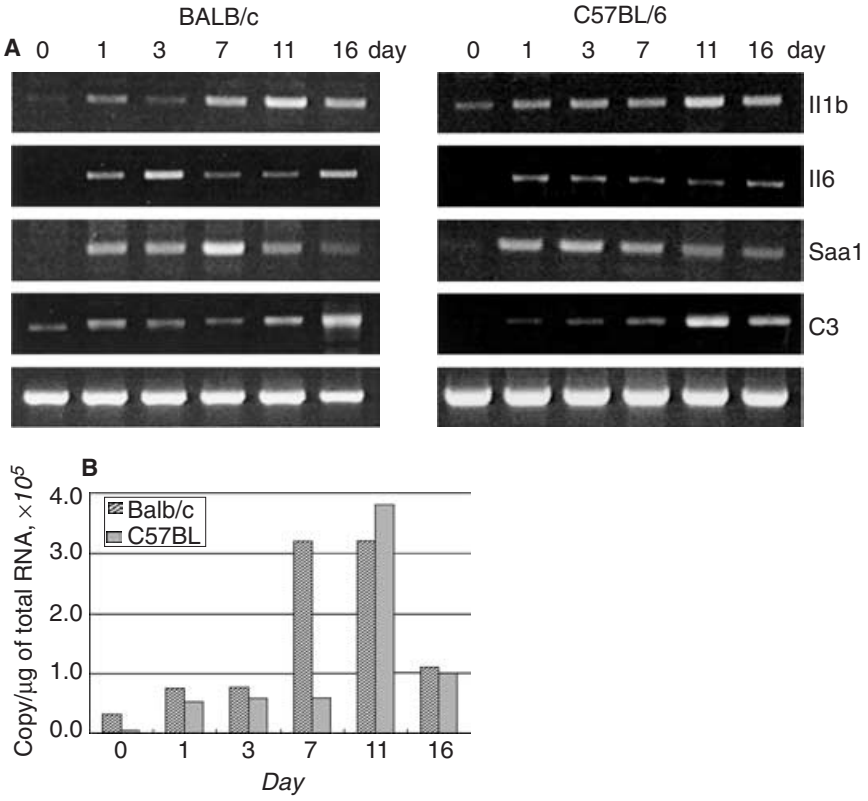


**Fig. 3. Reverse transcription-polymerase chain reaction (RT-PCR) and real-time PCR analysis on nuclear factor-κB (NF-κB) target genes.** (*A*) The transcript levels of NF-κB target genes (*IL-6, IL-1*β, *Saa1*, and C3), selected from Table 2, were analyzed by RT-PCR in both BALB/c and C57BL/6 mice. (*B*) Using real-time PCR method, the copy number of *IL-1*β was measured in both BALB/c and C57BL/6 mice.

downstream target molecules like CTGF [31]. Although our microarray result did not detect an increase of TGF-β1, the transcript was detected at late phase of the disease, as observed using ELISA and RT-PCR. The presence and action of TGF-β1 was indirectly uncovered in our microarray data through discovering the up-regulation of target genes at late phase. These results support the previous notion that TGF-β1 leads to fibrogenic effects in inflammatory nephropathy. On the other hand, the expression of CTGF was expressed quite ahead of TGF-β1 within 24 hours after immune complex formation in our study. The expression of CTGF modulates tissue response at early stage of glomerulonephritis [31]. Even the early expression of CTGF in glomerular diseases can be used as a biomarker [32].

The disease progression of our model mice occurred so rapidly that they die within 3 weeks after the antibody injection. Because it might not be enough to recruit lymphocytes, we could detect local immune reactions mediated by mesangial cells (Table 1). Nonetheless, mesangial cell activation has been suggested to be a central response of inflammatory models of renal diseases and various human nephropathies [33, 34]. Immune complex deposition acutely triggered the circulating neutrophil activation to produce the cytokines for mesangial cells. Traf can mediate the inflammatory response to nuclei through NF-κB activation [35]. We could monitor the elevation of Traf1 message in mesangial cells within 24 hours in immunofluorescence staining. Although the role of Traf1 in NF-κB activation is still controversial [36, 37], it may be important to mediate mesangial response for NF-κB activation in this model.

We noticed many growth factors like EGF or IGF and ESTs without functional annotation were suppressed with progression of the disease, which might be a putative target for minimizing the progression to fibrogenic change (Supplement Data A). Another therapeutic approach may be antagonizing proinflammatory molecules like platelet-derived growth factor (PDGF) by using neutralizing antibodies, which have been proven to be effective in reducing proliferation in animal models [34]. If we have information regarding upstream targets governing proinflammatory molecules, we may be able to block intracellular signals simultaneously. Currently, we focused our attention to several transcription factors. The regulatory repertoire of transcription factor families appears to be pivotal for the modulation of gene expression. Numerous proinflammatory genes have regulation motifs for NF-κB [38, 39]. We listed the elevation of NF-κB target genes in our microarray data (Table 2). Since there is a close relationship between NF-κB and mediators of cell activation, it is possible that disruption of NF-κB activating pathways may effectively influence mesangial cell activation.

A large number of studies have made use of quantitative RT-PCR, serial analysis of gene expression

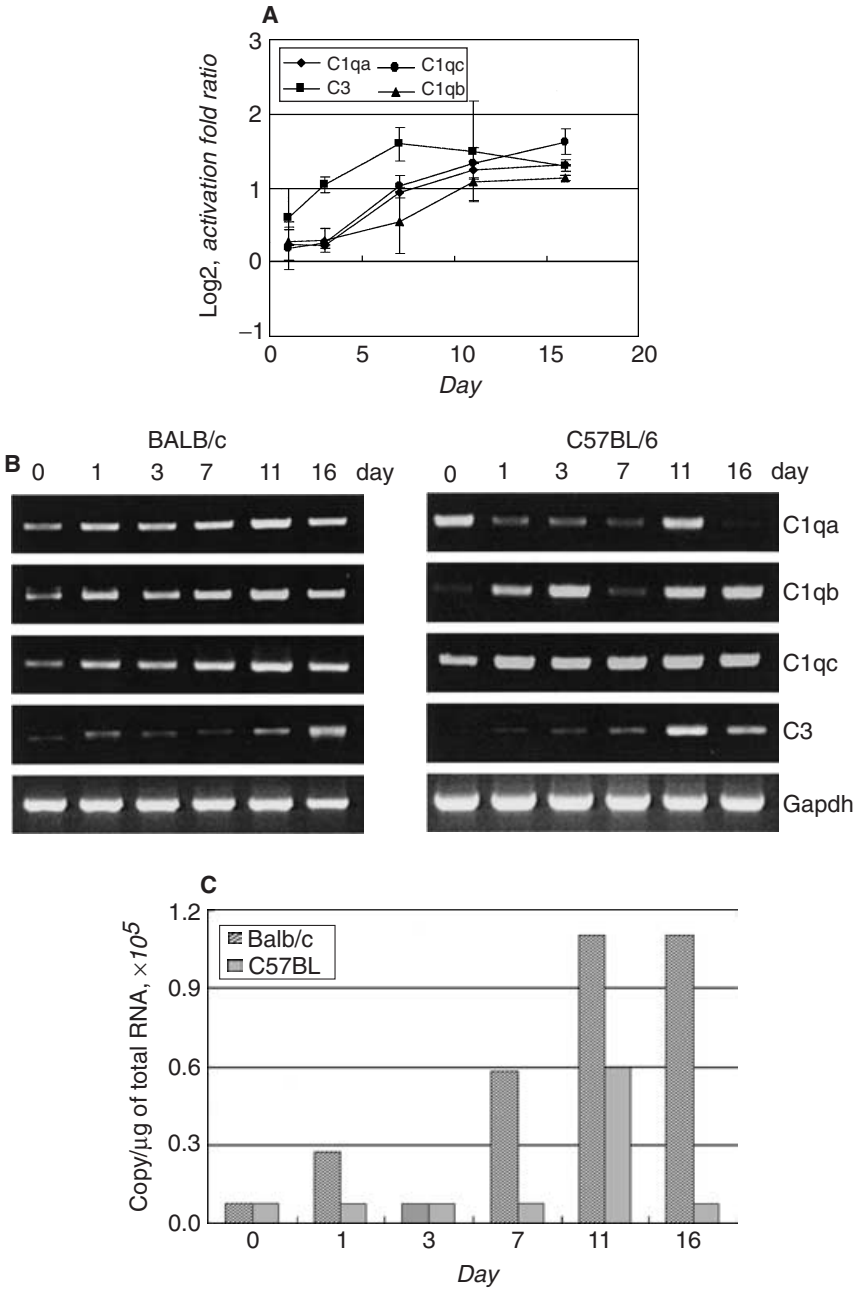


**Fig. 4. Increased expression of complement genes in anti-glomerular basement membrane (GBM) glomerulonephritis model.** (*A*) $Log_2$ transformed ratio of complement proteins in DNA microarray was plotted with standard deviation ($N = 3$) at each time point. (*B*) The levels of transcripts of *C1qα*, *C1qβ*, *C1qc*, and *C3* were analyzed by reverse transcription-polymerase chain reaction (RT-PCR) using total RNA from BALB/c and C57BL/6. (*C*) The copy number of C1qc transcript was measured by real-time PCR.

(SAGE), or single nucleotide polymorphism (SNP) to find biomarkers for prognosis or disease progression [4, 40, 41]. Microarray gene expression profiling might be used to determine disease markers and to understand pathogenesis [42]. Although not unique, our observations highlight the importance of subdividing the stages of glomerulonephritis. The detailed staging by gene expression profiles may enable scientists and clinicians to tailor therapeutic strategies by fine-tuning their regimen to the individual patient's disease stage. Additionally, current study as well as a variety of recent studies mentioned here validate data from previous studies on anti-GBM disease and provide important directions for further investigations. Application of the information obtained from this study is not confined to anti-GBM disease but expandable to most basic and clinical researches on progressive renal diseases.

## ACKNOWLEDGMENTS

The authors would like to thank our lab members for their inspiring ideas on this project. This work was supported by the IMT-2000 project (01-PJ11-PG9-01BT00A-0029) and BK21 project to W.-Y. P. The authors would also like to thank all the members in the laboratory for their contributions to this paper. The microarray data illustrated in this paper were submitted to the Gene Expression Omnibus (*http://www.ncbi.nlm.nih.gov/geo/*) under accession numbers GSM15078-GSM15092, GSE954-GSE958, and GSE969.

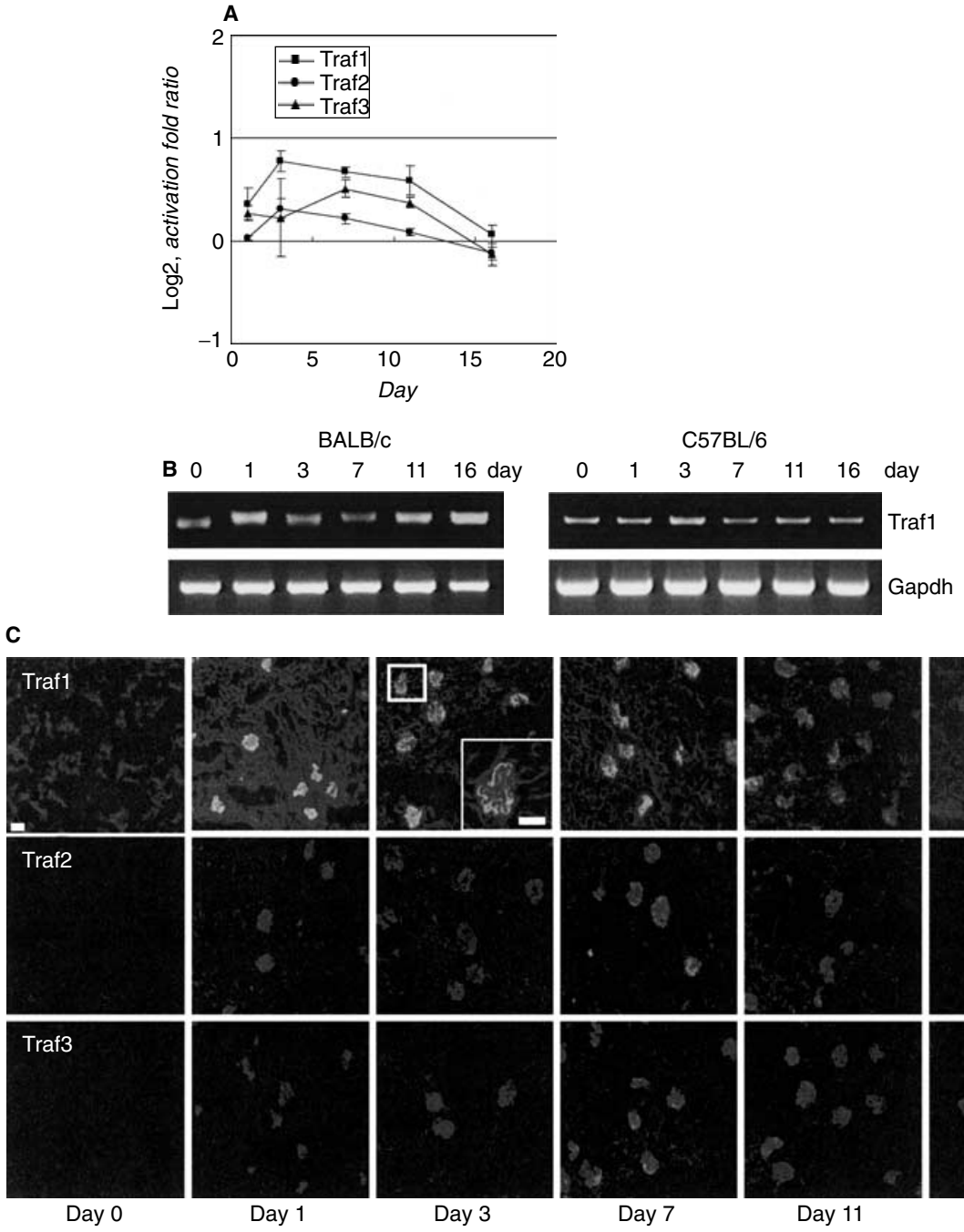


**Fig. 5. Induction of Traf1 in anti-glomerular basement membrane (GBM) glomerulonephritis model.** (*A*) Time-dependent expression profile of *Traf1*, *Traf2*, and *Traf3* genes were monitored using DNA microarray. Each log value represents an average of three replicate experiments from different animals with error bar displaying the standard deviation. (*B*) Using both BALB/c and C57BL/6 mice, the level of Traf1 mRNA were measured by reverse transcription-polymerase chain reaction (RT-PCR). (*C*) Immunofluorescence staining against *Traf1*, *Traf2*, and *Traf3* also showed changes in protein levels throughout the anti-GBM glomerulonephritis progression (100×).

*Reprint requests to Woong-Yang Park, M.D., Ph.D., Department of Biochemistry and Molecular Biology, Seoul National University College of Medicine, 28 Yongon-dong, Chongno-gu, Seoul 110–799, Korea. E-mail: wypark@snu.ac.kr*

## REFERENCES

1. Gerhold DL, Jensen RV, Gullans SR: Better therapeutics through microarrays. *Nat Genet* 32(Suppl):547–551, 2002
2. Butte A: The use and analysis of microarray data. *Nat Rev Drug Discov* 1:951–960, 2002
3. Shipp MA, Ross KN, Tamayo P, *et al*: Diffuse large B-cell lymphoma outcome prediction by gene-expression profiling and supervised machine learning. *Nat Med* 8:68–74, 2002
4. Hayden PS, El-Meanawy A, Schelling JR, Sedor JR: DNA expression analysis: Serial analysis of gene expression, microarrays and kidney disease. *Curr Opin Nephrol Hypertens* 12:407–414, 2003

5. Eikmans M, Baelde HJ, de Heer E, Bruijn JA: RNA expression profiling as prognostic tool in renal patients: Toward nephrogenomics. *Kidney Int* 62:1125–1135, 2002
6. Healy E, Brady HR: Role of tubule epithelial cells in the pathogenesis of tubulointerstitial fibrosis induced by glomerular disease. *Curr Opin Nephrol Hypertens* 7:525–530, 1998
7. Page R, Morris C, Williams J, *et al*: Isolation of diabetes-associated kidney genes using differential display. *Biochem Biophys Res Commun* 232:49–53, 1997
8. Yano N, Endoh M, Nomoto Y, *et al*: Phenotypic characterization of cytokine expression in patients with IgA nephropathy. *J Clin Immunol* 17:396–403, 1997
9. Yano N, Endoh M, Fadden K, *et al*: Comprehensive gene expression profile of the adult human renal cortex: Analysis by cDNA array hybridization. *Kidney Int* 57:1452–1459, 2000
10. Silverstein DM, Travis BR, Thornhill BA, *et al*: Altered expression of immune modulator and structural genes in neonatal unilateral ureteral obstruction. *Kidney Int* 64:25–35, 2003
11. Salant DJ, Cybulsky AV: Experimental glomerulonephritis. *Method Enzymol* 162:421–461, 1988
12. Kagami S, Border WA, Ruoslahti E, Noble NA: Coordinated expression of beta 1 integrins and transforming growth factor-beta-induced matrix proteins in glomerulonephritis. *Lab Invest* 69:68–76, 1993
13. Yamamoto T, Noble NA, Miller DE, Border WA: Sustained expression of TGF-β1 underlies development of progressive kidney fibrosis. *Kidney Int* 45:916–927, 1994
14. Peters H, Border WA, Noble NA: L-Arginine supplementation increases mesangial cell injury and subsequent tissue fibrosis in experimental glomerulonephritis. *Kidney Int* 55:2264–2273, 1999
15. Eberwine J: Amplification of mRNA populations using aRNA generated from immobilized oligo(dT)-T7 primed cDNA. *BioTechniques* 20:584–591, 1996
16. Huber W, Von Heydebreck A, Sultmann H, *et al*: Variance stabilization applied to microarray data calibration and to the quantification of differential expression. *Bioinformatics* 18(Suppl 1):S96–S104, 2002
17. Yang YH, Dudoit S, Luu P, Speed TP: Normalization for cDNA microarray data. *Technical Report* (*http://www.stat.berkeley.edu/users/terry/zarray/Html/normspie.html*), 2000
18. Wilk MB, Gnanadesikan R: Probability plotting methods for the analysis of data. *Biometrika* 55:1–17, 1968
19. Dwass M: Modified randomized tests for nonparametric hypotheses. *Ann Math Stat* 28:181–187, 1957
20. Storey JD, Tibshirani R: Statistical significance for genomewide studies. *Proc Natl Acad Sci USA*, 100:9440–9445, 2003
21. Kim JH, Ohno-Machado L, Kohane IS: Visualization and evaluation of clustering structures for gene expression data analysis. *J Biomed Inform* 35:25–36, 2002
22. Chung HJ, Kim MG, Park CH, *et al*: ArrayXPath: Mapping and visualizing microarray gene-expression data with integrated biological pathway resources using Scalable Vector Graphics. *Nuc Acids Res* 2004 (in press)
23. Nagase T, Uozumi N, Ishii S, *et al*: A pivotal role of cytosolic phospholipase A(2) in bleomycin-induced pulmonary fibrosis. *Nat Med* 8:480–484, 2002
24. O'Shea M, Miller SB, Finkel K, Hammerman MR: Roles of growth hormone and growth factors in the pathogenesis and treatment of kidney disease. *Curr Opin Nephrol Hypertens* 2:67–72, 1993
25. Doi T, Striker LJ, Gibson CC, *et al*: Glomerular lesions in mice transgenic for growth hormone and insulin-like growth factor-1. Relationship between increased glomerular size and mesangial sclerosis. *Am J Pathol* 137:541–552, 1990
26. Shinozaki M, Hirahashi J, Lebedeva T, *et al*: IL-15 a survival factor for kidney epithelial cells, counteracts apoptosis and inflammation during nephritis. *J Clin Invest* 109:951–960, 2002
27. Yamamoto T, Noble NA Cohen AH, *et al*: Expression of transforming growth factor-beta isoforms in human glomerular diseases. *Kidney Int* 49:461–469, 1996
28. Iwano M, Kubo A, Nishino T, *et al*: Quantification of glomerular TGF-β1 mRNA in patients with diabetes mellitus. *Kidney Int* 49:1120–1126, 1996
29. Gupta S, Clarkson MR, Duggan J, Brady HR: Connective tissue growth factor: Potential role in glomerulosclerosis and tubulointerstitial fibrosis. *Kidney Int* 58:1389–1399, 2000
30. Alcorta DA, Prakash K, Waga I, *et al*: Future molecular approaches to the diagnosis and treatment of glomerular disease. *Semin Nephrol* 20:20–31, 2000
31. Hishikawa K, Oemar BS, Nakaki T: Static pressure regulates connective tissue growth factor expression in human mesangial cells. *J Biol Chem* 276:16797–16803, 2001
32. Riser BL, Cortes P, Denichilo M, *et al*: Urinary CCN2 (CTGF) as a possible predictor of diabetic nephropathy: Preliminary report. *Kidney Int* 64:451–458, 2003
33. Johnson RJ: The glomerular response to injury: Progression or resolution? *Kidney Int* 45:1769–1782, 1994
34. Floege J, Grone HJ: Progression of renal failure: What is the role of cytokines? *Nephrol Dial Transplant* 10:1575–1586, 1995
35. Zapata JM, Reed JC: TRAF1: Lord without a RING. *Sci STKE* 133:PE27, 2002
36. Tsitsikov EN, Laouini D, Dunn IF, *et al*: TRAF1 is a negative regulator of TNF signaling enhanced TNF signaling in TRAF1-deficient mice. *Immunity* 15:647–657, 2001
37. Nolan B, Kim R, Duffy A, *et al*: Inhibited neutrophil apoptosis: Proteasome dependent NF-kappaB translocation is required for TRAF-1 synthesis. *Shock* 14:290–294, 2000
38. Baldwin ASJ: The NFκB and IkB proteins: New discoveries and insights. *Annu Rev Immunol* 14:649–681, 1996
39. Barnes PJ, Karin M: Nuclear factor-kB: A pivotal transcription factor in chronic inflammatory diseases. *N Engl J Med* 336:1066–1071, 1997
40. Ranieri E, Gesualdo L, Petrarulo F, Schena FP: Urinary IL-6/EGF ratio: A useful prognostic marker for the progression of renal damage in IgA nephropathy. *Kidney Int* 50:1990–2001, 2001
41. Kim YS, Kang D, Kwon DY, *et al*: Uteroglobin gene polymorphisms affect the progression of immunoglobulin A nephropathy by modulating the level of uteroglobin expression. *Pharmacogenetics* 11:299–305, 2001
42. Park WY, Hwang CI, Im CN, *et al*: Identification of radiation-specific responses from gene expression profile. *Oncogene* 21:8521–8528, 2002